

# Epidural electrical stimulation effectively restores locomotion function in rats with complete spinal cord injury

<https://doi.org/10.4103/1673-5374.290905>

Received: February 20, 2020

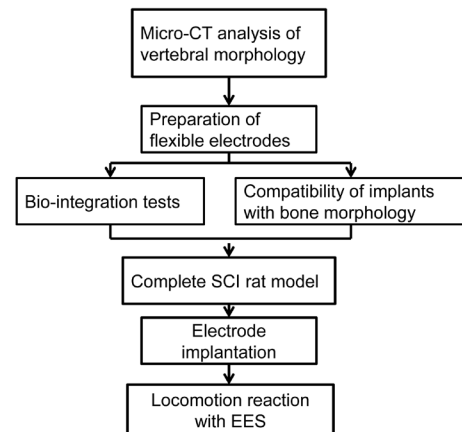
Peer review started: February 26, 2020

Accepted: April 26, 2020

Published online: September 22, 2020

Song Wang<sup>1,2</sup>, Li-Cheng Zhang<sup>2</sup>, Hai-Tao Fu<sup>3</sup>, Jun-Hao Deng<sup>2</sup>, Gao-Xiang Xu<sup>2</sup>, Tong Li<sup>4</sup>, Xin-Ran Ji<sup>2,\*</sup>, Pei-Fu Tang<sup>2,\*</sup>

**Graphical Abstract** Epidural electrical stimulation (EES) system can effectively restore the exercise capacity in rats with complete spinal cord injury (SCI), using three reasonably distributed hotspots and bursts of stimulus signals



## Abstract

Epidural electrical stimulation can restore limb motor function after spinal cord injury by reactivating the surviving neural circuits. In previous epidural electrical stimulation studies, single electrode sites and continuous tetanic stimulation have often been used. With this stimulation, the body is prone to declines in tolerance and locomotion coordination. In the present study, rat models of complete spinal cord injury were established by vertically cutting the spinal cord at the T8 level to eliminate disturbance from residual nerve fibers, and were then subjected to epidural electrical stimulation. The flexible extradural electrode had good anatomical topology and matched the shape of the spinal canal of the implanted segment. Simultaneously, the electrode stimulation site was able to be accurately applied to the L2–3 and S1 segments of the spinal cord. To evaluate the biocompatibility of the implanted epidural electrical stimulation electrodes, GFAP/Iba-1 double-labeled immunofluorescence staining was performed on the spinal cord below the electrodes at 7 days after the electrode implantation. Immunofluorescence results revealed no significant differences in the numbers or morphologies of microglia and astrocytes in the spinal cord after electrode implantation, and there was no activated Iba-1<sup>+</sup> cell aggregation, indicating that the implant did not cause an inflammatory response in the spinal cord. Rat gait analysis showed that, at 3 days after surgery, gait became coordinated in rats with spinal cord injury under burst stimulation. The regained locomotion could clearly distinguish the support phase and the swing phase and dynamically adjust with the frequency of stimulus distribution. To evaluate the matching degree between the flexible epidural electrode (including three stimulation contacts), vertebral morphology, and the level of the epidural site of the stimulation electrode, micro-CT was used to scan the thoracolumbar vertebrae of rats before and after electrode implantation. Based on the experimental results of gait recovery using three-site stimulation electrodes at L2–3 and S1 combined with burst stimulation in a rat model of spinal cord injury, epidural electrical stimulation is a promising protocol that needs to be further explored. This study was approved by the Animal Ethics Committee of Chinese PLA General Hospital (approval No. 2019-X15-39) on April 19, 2019.

**Key Words:** behavior; injury; model; neurological function; rat; recovery; regeneration; repair; spinal cord

Chinese Library Classification No. R459.9; R363; R364

<sup>1</sup>School of Medicine, Nankai University, Tianjin, China; <sup>2</sup>Department of Orthopedics, Chinese PLA General Hospital, Beijing, China; <sup>3</sup>Department of Orthopedics, The Affiliated Hospital of Qingdao University, Qingdao, Shandong Province, China; <sup>4</sup>Characteristic Medical Center of the Chinese People's Armed Police Force, Tianjin, China

\*Correspondence to: Xin-Ran Ji, MD, 18510622211@163.com; Pei-Fu Tang, MD, pftang301@163.com.

<https://orcid.org/0000-0002-6994-5008> (Xin-Ran Ji); <https://orcid.org/0000-0003-4279-1704> (Pei-Fu Tang)

**Funding:** This study was supported by the National Natural Science Foundation of China, Nos. 81601052 (to XRJ), 81520108017 (to PFT); the Beijing Nova Program of Science and Technology of China, No. 2018034 (to XRJ); the Beijing Municipal Science and Technology Project of China, No. D16100002816005 (to PFT); the Subsidiary of PLA Major Project of China, No. AWS17J004 (to PFT).

**How to cite this article:** Wang S, Zhang LC, Fu HT, Deng JH, Xu GX, Li T, Ji XR, Tang PF (2021) Epidural electrical stimulation effectively restores locomotion function in rats with complete spinal cord injury. *Neural Regen Res* 16(3):573-579.

## Introduction

Spinal cord injury (SCI) is a neurological trauma that affects approximately 347,000 individuals in the USA, with approximately 17,500 new cases occurring each year (Badhiwala et al., 2019; Collaborators, 2019). Restoring the voluntary control of paralyzed limbs is always a high priority for SCI patients with paraplegia or tetraplegia (Anderson, 2004; Hutson and Di Giovanni, 2019). Most researchers remain focused on the use of pharmacological agents (Anderson et al., 2018; Sun et al., 2019), stem cell treatments (Zhang et al., 2016; Assinck et al., 2017; Kim et al., 2018; Cofano et al., 2019; Shi et al., 2020), and other regenerative methods (Koffler et al., 2019; Ni et al., 2019; Ren et al., 2019; Tsintou et al., 2020) to regenerate damaged neural tissue, but the degree of motor recovery with these methods remains limited.

After SCI, communication between the supraspinal centers and spinal circuits is interrupted by injury, but neural structures below the injury level remain intact (David et al., 2019; Urbin et al., 2019; Yuan et al., 2019). Theoretically, it is possible to restore innervation function if proper stimulus is applied (Kjell and Olson, 2016; Badner et al., 2017). In recent years, epidural electrical stimulation (EES), a neuromodulation technique, has shown promising therapeutic potential to restore limb mobility by reactivating surviving neural circuits after SCI (Angeli et al., 2018; Gill et al., 2018; Calvert et al., 2019).

Originally, EES was developed to treat chronic pain (Epstein and Palmieri, 2012; Balki et al., 2019), and many studies have used the same concepts and protocols for the treatment of SCI, such as the use of nonspecific stimulation, stimulation that is restricted to single regions, and continuously delivered stimulation. However, these stimulation protocols have been demonstrated to have many disadvantages in SCI treatment, making it difficult to obtain reliable results (Formento et al., 2018). Not only does the body have poor tolerance to continuous stimulation, but it can also be difficult to obtain coordinated and satisfactory gait movements (especially for fine limb movements, such as foot movements) (Jackson and Zimmermann, 2012; Wenger et al., 2016). Evidence from computer modeling (Rattay et al., 2000; Capogrosso et al., 2013; Wenger et al., 2014), animal studies (Gerasimenko et al., 2006, 2007; Wenger et al., 2016), and clinical trials (Angeli et al., 2018; Gill et al., 2018; Wagner et al., 2018) shows that applying spatiotemporal burst stimulations can achieve better recovery of motor performance. However, a dilemma remains: continuously increasing the complexity of EES configuration schemes does not always mean that the results will improve. In fact, complicated EES protocols have limited progress in the research and application of EES. An ideal EES protocol would specifically reactivate motor pools or even specific motor neurons to achieve precise muscle activation and control of movements. However, anatomical results suggest that the motor pools innervating hindlimb muscles are highly overlapped along the rostrocaudal axis in ventrolateral regions of the spinal cord (Mohan et al., 2015). The L2–3 and S1 segments have been suggested as possible locations where stimulation may be effective enough to recruit extensor and flexor hotspots, thus restoring locomotion (Hunter and Ashby, 1994; Gerasimenko et al., 2006; Wenger et al., 2016).

Based on these previous data and biological principles, we hypothesized that, to facilitate movement after SCI, three distributed hotspot electrodes and interleaved delivered burst stimulation may be used to effectively reproduce patterns of motor neuron activation. Furthermore, this configuration of EES avoids involving complex regulation parameters, so this model can be used in future research of evidence-based EES strategies. This study therefore investigated the effects of a new EES model on restoring motor ability in a rat model of complete SCI.

## Materials and Methods

### Animals

A total of 40 female Sprague-Dawley rats with initial weights of 180–240 g, aged 6–8 weeks, were provided by the Laboratory Animal Center of Chinese PLA General Hospital [animal license no. SYXK (Jun) 2017-0019]. All rats were acclimated to standard housing, in which they had food and water available *ad libitum*, with a constant temperature of 22°C, 45% humidity, and a 12-hour light/dark cycle. All invasive experimental procedures were performed using anesthesia to minimize pain. The study was approved by the Medical Ethics Committee of the Chinese PLA General Hospital (approval No. 2019-X15-39) on April 19, 2019.

The rats were divided into three groups: the vertebral measurement group ( $n = 22$ ), the inflammation analysis group ( $n = 8$ ), and the EES group ( $n = 10$ ). In the vertebral measurement group, rats were further subjected to micro-CT scanning ( $n = 4$ ), anatomical measurement ( $n = 10$ ), and implantation ( $n = 8$ ). In the inflammation analysis group, the eight rats were randomly assigned to either the sham group ( $n = 4$ ) or the implantation group ( $n = 4$ ). On postoperative day 7, the rats were sacrificed to determine the bio-integration of implants. In the EES group, rats were subjected to electrode implantation. On postoperative day 3, the rats received EES and locomotor performance assessments.

### Flexible stimulation implant and hardware

The flexible stimulating electrodes were obtained from the Key Laboratory of Image Processing and Intelligent Control of Education Ministry, Huazhong University of Science and Technology, Wuhan, China (Zhou et al., 2012). The implant was manufactured with a flexible circuit board technique and had anatomical topologies for locating and stabilizing the implant on the dorsal epidural surface of the spinal cord. For the stimulation of epidural spinal cord regions, the whole length of the implant contained stimulation and fixation regions, and the three 1 mm round golden contacts were separated by an 8 mm center-to-center distance from one another. The impedance of the electrode-lead system was measured previously, at approximately 21 k $\Omega$  at 100 Hz in 0.9% saline and 22 k $\Omega$  *in vivo* (Zhou et al., 2012). The leads were made of silver wire and coated with Teflon (A-M System Inc., Sequim, WA, USA). To avoid mechanical fractures resulting from rat muscle friction, the leads were protected by medical silicon tubes. The designed flexible stimulating electrodes targeting flexor and extensor hotspots were placed in the epidural space during the surgical procedure and were fixed using dental cement to the appropriate location.

A stimulus generator (CereStim R96; Blackrock Microsystems, UT, USA) was used. The programmable 96-channel neural stimulator simultaneously sent 16 channels of electrical stimulation signals, with output range: current 1  $\mu$ A–10 mA, voltage  $\pm$ 9.5 V. The bipolar pulse function was specifically suited to the stimulation of neurons with implanted electrodes.

### SCI and implantation procedures

General surgical procedures of SCI have been described previously (Courtine et al., 2008; Lavrov et al., 2008; Capogrosso et al., 2018). Briefly, rats were anesthetized with isoflurane in oxygen-enriched air (1–2%) and an incision was made in the middle of the back, centered on the T8 vertebral level. After the paraspinal muscles were isolated and the T8 lamina was removed, the spinal cord was exposed. A transection injury was performed to completely cut the spinal circuits (representing the spinal cord between T8 and T9 levels) that control hindlimb movement. If the spinal cord tissue was completely disrupted, the model establishment was considered to be successful (**Figure 1**). After adequate hemostasis, the incision was carefully sutured. Manual

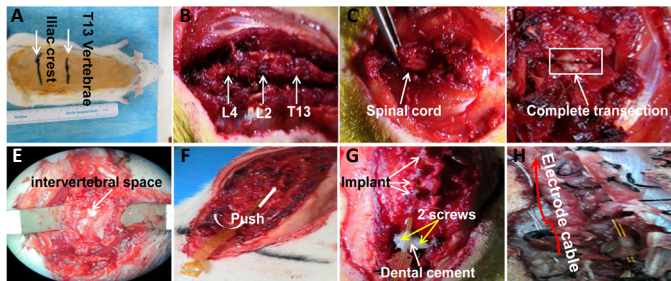


**Figure 1 | Implantation of flexible epidural electrodes.** (A) Sterilizing the surgical field and identifying T13 and the iliac crest; (B) exposing the vertebral body and intervertebral space; (C) performing laminectomies to expose the spinal cord; (D) performing complete transection of the spinal cord; (E) exposing the intervertebral space to prepare the insertion of the implant; (F) inserting the flexible implant; (G) fixing the implant using dental cement and screws; (H) suturing muscles and fixing electrode cables.

pressure on the rat bladder was conducted twice daily to assist urination.

To implant the flexible electrode, the L4–5 intervertebral space was identified as the entry site. Partial laminectomies were performed to expose the central intervertebral space of T12–L4. The flexible electrode was gently pushed above the midline of the dura mater and the position was adjusted through the exposed intervertebral space. The implant position was further adjusted according to the hindlimb movements that were elicited under the following conditions: short burst stimulation parameters (4 pulses at 40 Hz, 200  $\mu$ s pulse-width) and suspended posture. After the implants were inserted, two holes were drilled in the L4 vertebral body and two stainless steel screws (diameter 1 mm) were inserted and fixed with dental cement (**Figure 1**). Small holes at the distal implant were also used to help suture the implant onto the tendon and muscles. After adequate hemostasis, the muscles and skin were sutured. During recovery from anesthesia, the animals were placed in a temperature- and humidity-controlled chamber.

### Immunofluorescence and quantitative analyses

To evaluate the inflammatory response, spinal cord samples were taken on day 7 after the electrode implantation. The implanted and sham-operated rats were sacrificed to perform immunofluorescent staining (four rats per group). Rats were anesthetized and rapidly perfused transcardially with 0.1 M phosphate-buffered saline (PBS) followed by 4% paraformaldehyde. L4–5 segments under the implants were collected to determine the inflammatory reaction. Spinal cord samples were fixed in 4% paraformaldehyde overnight, followed by cryoprotection in 30% sucrose solution at 4°C. After the samples sank, the spinal cord was sectioned on a cryostat microtome at 25  $\mu$ m thickness. For immunofluorescent staining, the sections were blocked with PBS containing 0.4% Triton X-100 and 10% goat serum for 2 hours at room temperature. After an overnight incubation with primary antibodies at 4°C, the samples were washed three times with PBS for 10 minutes. After being incubated at room temperature for 2 hours with secondary antibodies, sections were stained with DAPI (Solarbio, C0060, Beijing, China) to visualize nuclei, followed by two washes in PBS.

The neuroinflammatory markers GFAP (reactive astrocytes) and Iba-1 (reactive microglia/macrophages) were stained to quantify the inflammatory reaction. The primary antibodies were anti-GFAP (1:1000, chicken polyclonal; Abcam, London, UK) and anti-Iba-1 (1:1000, rabbit polyclonal; Kanagawa Prefecture, Wako, Japan). The secondary antibodies were Alexa Fluor 647 (anti-chicken IgY, Abcam) and Alexa Fluor 488 (anti-rabbit IgG, ab150073, Abcam). Confocal images were captured using a confocal microscope (Leica, Wetzlar,

Germany). Three-dimensional (3D) reconstructions were made using Leica image processing software and Imaris software (Bitplane, Zurich, Switzerland).

The total numbers of immunolabeled microglia (Iba1<sup>+</sup>) and astrocytes (GFAP<sup>+</sup>) were counted at 20 $\times$  magnification (1392  $\times$  1040 pixels) from images obtained using a PerkinElmer Vectra Slide Scanner (PerkinElmer, MA, USA). The measured areas were identified as the proportional area (600  $\times$  600 pixels) in the spinal dorsal horn. A total of 16 representative images were assessed (two sections per rat, one section from each region-of-interest field). Immunolabeled cells with a DAPI-stained nucleus were then manually counted using ImageJ software (version 1.52a; NIH, Bethesda, MD, USA). All quantitative analysis was performed blinded to animal identities.

### Micro-CT

To evaluate the matching degree of the implants with vertebral morphology, micro-CT scanning was performed before implantation. High-resolution images were acquired using a Micro-CT (PerkinElmer, Control Version 3.0). During the scan, animals were kept under anesthesia to reduce motion blurriness and artifacts. Using image analysis software (Mimics Research software, NV, USA), 3D global models of vertebrae were reconstructed and anatomical data were measured, including the vertebral body length (VBh), spinal canal depth (SCd), spinal canal width (SCw), spinal canal area (SCa), and spinal canal perimeter (SCp). To quantitatively measure spinal anatomy, anatomical landmarks were identified as described previously in human and animal studies (Panjabi et al., 1991; Flynn and Bolton, 2007; Jaumard et al., 2015). Briefly, VBh was defined as the length from the upper endplate to the inferior aspect; SCd was defined as the maximum length of the spinal canal along the anteroposterior direction; and SCw was defined as the maximum lateral dimensions of the normal spinal canal to midline (**Figure 2**). The length of multivertebrae was measured along the medial dorsal wall of the spinal canal containing the vertebrae and discs.

### EES and gait analysis

On postoperative day 3, the rats received EES. Rats with inserted flexible implants were trained for 20 minutes a day. All animals were suspended to achieve the optimal assisted unloaded condition, and rehabilitation was conducted on a treadmill (1 m/min). After the rats had adapted to the training state (no obvious fear or attempts to escape), electrical stimulation currents were delivered using the stimulus generator. Four fiducial markers were identified on the iliac crest (hip), knee, ankle, and limb endpoint during the training. The movement indicators of hind limbs, including ankle angle, foot-to-ground height, and toe movement distance, were recorded by a camera placed parallel to the side of the treadmill. Performance was analyzed using Kinovea (version, 0.8.15, <https://www.kinovea.org/>). The stimulation parameters for epidural electrical stimulation were set as: 40 Hz, 100–900  $\mu$ A, biphasic rectangular pulses, 200  $\mu$ s pulse-width, and 900 ms interval.

### Statistical analysis

Data were obtained as the average values from each rat and are expressed as the mean  $\pm$  SEM, unless specified otherwise. Student's *t*-test and one-way analysis of variance were used to analyze the significance of normally distributed data using Prism 7 software (GraphPad, San Diego, CA, USA). Tukey's *post hoc* test was performed when multiple comparisons were needed after one-way analysis of variance. A value of *P* < 0.05 was considered statistically significant.

## Results

### Vertebral morphological data

To evaluate the matching degree of the implant with rat

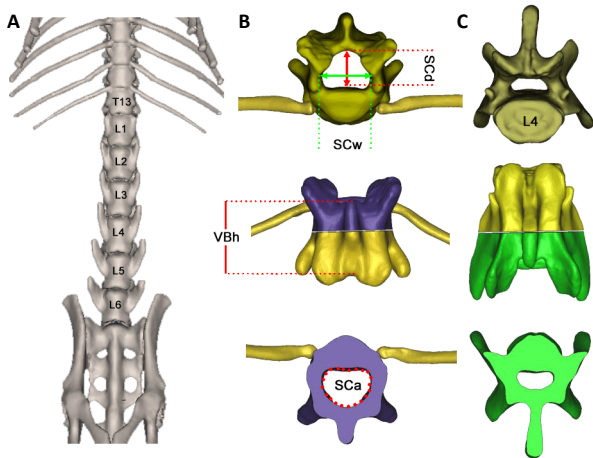


**Figure 2 | Micro-CT scanning and 3D reconstruction of thoracic and lumbar vertebrae in Sprague-Dawley rats.**

(A) The whole view of the T12–L6 vertebral body on the abdomen view; the VBh increases caudally. (B, C) 3D models of the T13 and L4 vertebrae were reconstructed and anatomical data were measured along the axial view. The reconstructed 3D vertebrae were separated from the middle for parameter measurements (the purple part represents the upper part of the thoracic body, while the green part represents the lower part of the lumbar body). 3D: Three-dimensional; VBh: vertebral body length; SCa: spinal canal area; SCd: spinal canal depth; SCw: spinal canal width.

vertebral morphological structures, we first measured the anatomical data of vertebrae T12–L6 in healthy rats. We also analyzed the matching degree of the implant using micro-CT and anatomical measurements (data not shown). Four rats underwent micro-CT scanning to measure the VBh, SCd, SCw, SCa, and SCp (**Table 1**). Images revealed that the whole length of T12–L6 was  $50.00 \pm 0.49$  mm. The length of the superior border of the T12–L2 vertebrae, corresponding to the hotspot distribution range that targeted hindlimb muscles, was  $16.52 \pm 0.45$  mm. The designed stimulating electrodes were therefore exactly matched with the range that could obtain accurate stimulating outcomes. The VBh increased caudally, and was significantly greater at L4 than at T12–L2 and L6 (**Figure 3**;  $P < 0.05$ ).

Unlike the trend for VBh variation, both the SCw and SCd generally decreased caudally (**Table 1**). In the lumbar spine, the SCw decreased 41.59% from L1 to L6 ( $P < 0.0001$ ). In addition, the SCw, SCd, and SCa at T13 were significantly greater than at L2–L6 ( $P < 0.05$ , **Figure 3**). The three maximum SCw values were  $3.24 \pm 0.04$  mm,  $3.48 \pm 0.07$  mm, and  $3.39 \pm 0.08$  mm at T12, T13, and L1, respectively. The three vertebral positions contained stimulating electrodes, and the anatomical morphology ideally contained the designed implants. The SCd, SCa, and SCp of L4 were  $1.28 \pm 0.09$  mm,  $2.92 \pm 0.08$  mm<sup>2</sup>, and  $6.92 \pm 0.15$  mm, respectively. These values decreased by 17.95%, 20.22%, and 8.22%, respectively, and were significantly lower than those at T12–L2 ( $P < 0.0001$ ). The vertebral body at L4 was greater than at T12–L2 and L6. From these data, the “safe operating position” was chosen for the flexible implant entry points, followed by fixation with screws and bone cement. These data demonstrate that the implant dimensions were compatible with the bone morphology.

### Bio-integration of the flexible implants

The bio-integration of the flexible implants was investigated by evaluating the inflammatory reaction and glial reactive hyperplasia in spinal cord segments below the implants. The numbers and cellular morphologies of neuro-inflammatory cells were examined by staining sections with GFAP (a marker of reactive astrocytes) and Iba-1 (a marker of reactive microglia and potential bone marrow-derived macrophages).

No inflammatory changes were observed after 1 week of

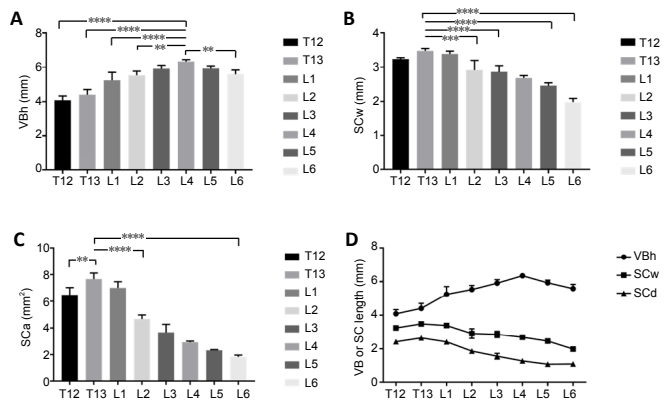


**Figure 3 | Quantification of T12–L6 vertebral anatomical parameters.**

(A–C) Comparison of morphological data among the T12–L6 vertebrae: VBh increased and was significantly greater at L4 (A); SCw (B) and SCd (C) generally decreased caudally and were significantly greater at T13. (D) Variation trends of VBh, SCw, and SCd. The SCd and SCw at L4 were significantly smaller than those at T12–L2, and the VBh at L4 was greater than that at T12–L2 and L6. Data are expressed as the mean  $\pm$  SEM ( $n = 4$ ; one-way analysis of variance followed by Tukey’s *post hoc* test). \*\* $P < 0.01$ , \*\*\* $P < 0.001$ , \*\*\*\* $P < 0.0001$ . SCa: Spinal canal area; SCd: spinal canal depth; SCw: spinal canal width; VBh: vertebral body length.

**Table 1 | Anatomical data (mm) of the T12–L6 vertebral bodies**

Segment of spinal cord	VBh	SCw	SCd	SCa	SCp
T12	4.08 $\pm$ 0.25	3.24 $\pm$ 0.04	2.42 $\pm$ 0.14	6.48 $\pm$ 0.55	9.53 $\pm$ 0.57
T13	4.40 $\pm$ 0.30	3.48 $\pm$ 0.07	2.64 $\pm$ 0.07	7.67 $\pm$ 0.45	10.13 $\pm$ 0.31
L1	5.24 $\pm$ 0.46	3.39 $\pm$ 0.08	2.41 $\pm$ 0.04	7.01 $\pm$ 0.46	9.89 $\pm$ 0.32
L2	5.53 $\pm$ 0.24	2.91 $\pm$ 0.29	1.86 $\pm$ 0.12	4.67 $\pm$ 0.30	8.33 $\pm$ 0.22
L3	5.91 $\pm$ 0.21	2.86 $\pm$ 0.19	1.56 $\pm$ 0.17	3.66 $\pm$ 0.61	7.54 $\pm$ 0.63
L4	6.35 $\pm$ 0.11	2.68 $\pm$ 0.07	1.28 $\pm$ 0.09	2.92 $\pm$ 0.08	6.92 $\pm$ 0.15
L5	5.93 $\pm$ 0.16	2.46 $\pm$ 0.08	1.09 $\pm$ 0.11	2.32 $\pm$ 0.05	6.22 $\pm$ 0.21
L6	5.58 $\pm$ 0.26	1.98 $\pm$ 0.11	1.10 $\pm$ 0.02	1.83 $\pm$ 0.13	5.43 $\pm$ 0.30

Data are expressed as the mean  $\pm$  SEM ( $n = 4$ ). SCa: Spinal canal area; SCd: spinal canal depth; SCp: spinal canal perimeter; SCw: spinal canal width; VBh: vertebral body length.

flexible epidural electrode implantation. Astrocytes in the two groups showed spider-like morphology, with normal, small nuclei and delicate fibrillary cytoplasm (**Figure 4**). There were no hypertrophic astrocytes (characterized by a ballooned appearance) or short thickened processes, and there were occasionally multiple nuclei. Microglia showed a resting phenotype characterized by a ramified morphology. There were no differences in phagocytic microglia (characterized by short and poorly ramified processes of different thicknesses around swollen cell bodies) concentrations between the two groups. Using high-resolution cell shape analysis, we did not observe abnormalities in microglia-like spherical, rod, or amoeboid shapes in the implantation group (**Figure 4**).

In the regions of interest, there were no significant differences in the numbers or fluorescence intensities of immunolabeled microglia (Iba1<sup>+</sup>) or astrocytes (GFAP<sup>+</sup>) between the two groups ( $P > 0.05$ ; **Figure 4**). These results indicate that the spinal implants had a negligible impact on the inflammatory environment of tissue under the implant.

### Locomotion after complete SCI

After SCI, all animals lost the motor ability of their hindlimbs both on the ground and on the treadmill (**Figure 5**). Serotonergic replacement therapy alone did not improve locomotion in the SCI rats. However, EES treatment led to the effective recovery of hindlimb motor ability on the treadmill. To quantify performance stimulated by different current parameters, we tested a stimulation range from 100–900

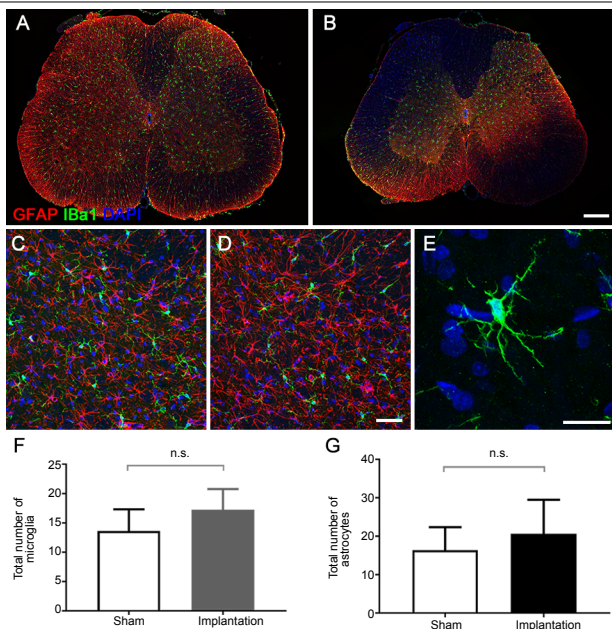


**Figure 4 | Morphology and quantification of astrocytes and microglia in epidural electrical stimulation models.**

(A, B) Confocal immunofluorescence images. The distribution of astrocytes (GFAP, red) and microglia (Iba-1, green) in the spinal cord sections below the implant (B) or at a similar level in the sham model (A) (confocal microscopy; original magnification: 200 $\times$ ). (C–E) Magnification of the confocal immunofluorescence images in the dorsal horn area. The morphology of astrocytes (GFAP, red) and microglia (Iba-1, green, white arrows) in the sham (C) and implantation (D) groups (confocal microscopy; original magnification: 400 $\times$ ). (E) Microglia in the implantation group showed a resting phenotype characterized by a ramified morphology. (F, G) Quantification of the total number of microglia (F) and astrocytes (G) in the region of interest (arrows). Data are expressed as the mean  $\pm$  SEM ( $n = 4$ ; Student's  $t$ -test). Scale bars: 300  $\mu$ m (B), 50  $\mu$ m (D), and 20  $\mu$ m (E). GFAP: Glial fibrillary acidic protein; Iba-1: ionized calcium-binding adaptor molecule 1; n.s.: not significant.

$\mu$ A. Results indicated that the most satisfactory locomotion outcome was obtained using a 600  $\mu$ A stimulation parameter. Ankle angle was an important evaluation indicator when using the treadmill. Our data showed that 100–400  $\mu$ A stimulation was not able to maintain a satisfactory locomotion performance. The rat ankle angles were poor at these stimulation parameters, meaning that the rats' feet were actively off the ground (Figure 5). At 200  $\mu$ A stimulation, the ankle angle results showed a central trend. However, using the 600  $\mu$ A condition, the angle was distinctly changed during gait. Under the 900  $\mu$ A condition, the angle induced a slightly abnormal movement of the abdominal muscles, but did not significantly elevate the locomotion performance of SCI rats. These data indicated that, in the present EES system (three hotspot electrodes, 40 Hz, biphasic rectangular pulses), 600  $\mu$ A achieved an effective locomotion reaction on the treadmill.

## Discussion

Promising therapeutic outcomes of EES in rodent, feline, and nonhuman primate models, as well as in SCI patients, have demonstrated the advantages of neuromodulation technologies for the treatment of SCI (Wenger et al., 2016; Schiavone et al., 2018; Wagner et al., 2018; Darrow et al., 2019; Zheng et al., 2020). However, in the absence of a conceptual framework, many EES protocols still use tonic stimulation (with nonspecific positions and continuous stimulation), which make it difficult to maintain satisfactory motor performance (Formento et al., 2018). Based on biological principles and data from previous research, we developed an EES protocol that used three relatively distributed hotspot electrodes combined with burst-delivered stimuli. This EES protocol was able to reliably reproduce locomotion ability by reactivating

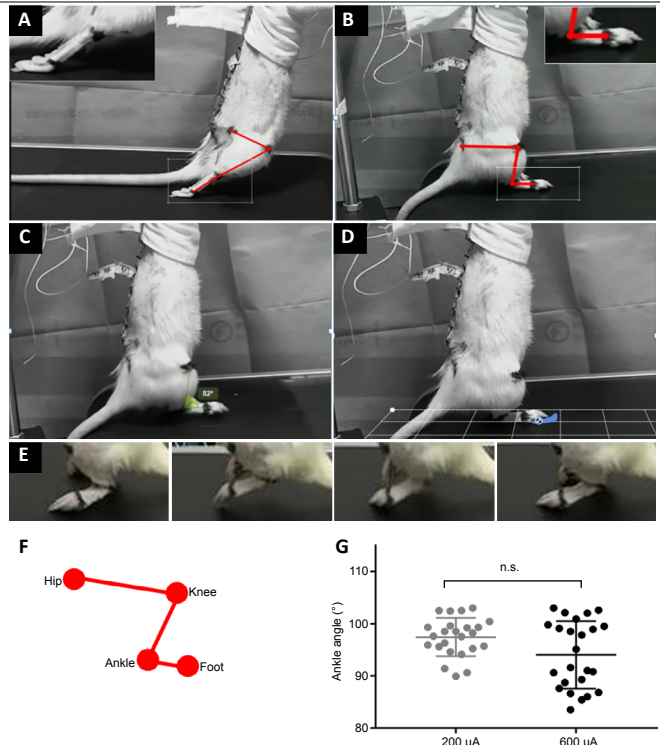


**Figure 5 | Locomotion under epidural electrical stimulation in rats with complete spinal cord injury (SCI).**

(A) Locomotion reaction of the hindlimbs of SCI rats on a treadmill without stimulation. (B) Hindlimb posture and marker positions at the beginning of stimulation. (C–E) Gait analysis of the hindlimb during epidural electrical stimulation: ankle angle (C), distance of the ends of toes (D), and step height (E). (F) Illustration of the fiducial markers: iliac crest (hip), knee, ankle, and limb endpoint (foot). (G) Quantification of the ankle angle with 200  $\mu$ A and 600  $\mu$ A stimulation currents. Data are expressed as the mean  $\pm$  SEM ( $n = 10$ ; Student's  $t$ -test). n.s.: Not significant.

the motor pools of rats with complete SCI, but avoided an overly complicated configuration.

In the present study, the designed flexible electrodes were implanted into a rat model of complete SCI, and the matching degree, bio-integration, and locomotion reaction of EES were assessed. Our results indicated that the dimensions of the designed flexible electrodes were compatible with rat bone morphology, and had a negligible impact on the inflammatory environment of spinal cord tissue. In the present EES system (three hotspot electrodes, 40 Hz, biphasic rectangular pulses), the protocol effectively restored locomotion reaction on the treadmill.

The most common clinical type of SCI is an incomplete injury, where some ascending and descending axons survive the injury but are functionally silent (Eckert and Martin, 2017; Karunakaran et al., 2019; Li et al., 2019; Yokota et al., 2019). In the present study, we did not choose an incomplete contusion model, but rather used a complete transection model to exclude the interference of remaining nerve fibers as much as possible. Our results showed that the SCI rats completely lost their hindlimb motility, both in the resting state and on the treadmill. A complete SCI model, such as the one used in the current study, allows for better evaluation of the EES activation of surviving neural circuits that innervate lower limb muscles. EES is often used to control chronic pain, including that of failed back surgery syndrome and complex regional pain syndrome, and is well recognized as a safe and effective therapeutic method (Moir, 2009; Kapural et al., 2010; Epstein and Palmieri, 2012). In addition, many studies have also used a single stimulation area method to treat SCI. Evidence from computer simulations (Capogrosso et al., 2013), animal studies (van den Brand et al., 2012), and clinical trials (Angeli

et al., 2018; Gill et al., 2018) have revealed that alternate stimulation at multiple epidural sites can better restore hindlimb movements after SCI. Thus, in the present study, we used three electrodes distributed over the epidural space instead of a single or nonspecific stimulation site. Our results showed that this model can achieve good gait movement through its multi-site alternating stimulation protocols. The mechanisms by which EES restores locomotion are: (1) activation of central pattern-generating networks (Danner et al., 2015; Young, 2015); (2) direct stimulation of motor neuron pools (Angeli et al., 2014); (3) indirect transfer of the stimulus signal to motor pools through proprioceptive fibers in dorsal roots (Lavrov et al., 2008; Wenger et al., 2014); and (4) altering spinal cord excitability to a level that enables sensory information to become a source of motor control (Edgerton et al., 2008; Harkema et al., 2011).

In contrast to EES protocols, intraspinal stimulation is a technique in which the electrodes penetrate motor pool locations to directly evoke functional motor responses (Saltiel et al., 2001; Mushahwar et al., 2004; Sunshine et al., 2013; Sharpe and Jackson, 2014). Although intraspinal stimulation may have theoretical advantages, in that it requires less current and produces more accurate motor responses, the high risk of electrode displacement, infection, and glial hyperplasia of chronically implanted electrodes all limit its application (Jackson and Zimmermann, 2012; Jackson, 2016). Many studies have proposed that muscle synergies, engaging a set of motor primitives, are the main pattern of electrical stimulation (Bamford et al., 2005; Moritz et al., 2007; Borrell et al., 2017). The spinal cord motor pools that innervate hindlimb muscles are highly overlapped along the rostrocaudal axis in the ventrolateral location (Gonzalez et al., 2013; Mohan et al., 2015). The L2–3 and S1 segments have been suggested as electrode locations that might effectively recruit extensor and flexor hotspots to restore locomotion (Wenger et al., 2016). The origins of rat L2 nerve roots arise at the level of the T12 vertebrae caudally, while those of the L3 arise at the level of the T13 vertebrae, and those of the S1 arise approximately at the level of the L2 superior border of the vertebra (Padmanabhan and Singh, 1979). These data suggest that, compared with attempts that target highly specific motor pools or neurons, restoring a range of specific and synergistic hindlimb movements may be useful in the development of EES therapeutic strategies for SCI patients.

Our results indicated that, with reasonable distribution of the hotspots, electrodes targeted at the L2–3 and S1 segments effectively reactivated the motor pools that innervate hindlimb muscles. The present configuration protocol not only focused on how to effectively reproduce locomotion after SCI, but also avoided the use of complex regulation parameters. Unlike in animal models, EES in humans usually needs to be combined with rehabilitation programs to recover independent, weight-bearing locomotion. As mentioned earlier, it is difficult to design complex electrodes and auxiliary equipment with precise stimulation parameters in the short term. We therefore reasoned that flexible epidural implants targeting the L2–3 and S1 segments would engage hindlimb muscles. Considering the importance of flexibility to reduce mechanical friction and inflammatory responses in the spinal cord, the present implants were manufactured with a flexible circuit board, could be placed in a dorsal site, and did not cause any inflammatory changes in the spinal cord tissue. The present flexible implants had three round golden contacts with a diameter of 1 mm, separated at an 8 mm center-to-center distance on the electrode. The three distributed electrodes were optimally located on the hotspots and successfully reproduced the electrical stimulation results. The use of a relatively small number of electrodes reduces technological challenges and theoretically has sufficient potential to reactivate hotspots innervating the hindlimb muscles.

We hope that this model supports the development of EES therapeutic strategies without complex regulation parameters and devices. However, there were some limitations in the current study. Because it was an EES protocol study, a more extensive range of bio-markers, such as SMI31 (axonal expression), neuronal markers, and cleaved caspase-3, were not included, and regeneration after SCI was therefore not evaluated. Other markers that reflect microglia and macrophage activation, such as CD68, were also not included in this study.

Although the development of EES still faces serious challenges, several EES protocols are currently moving from the laboratory to preliminary clinical trials (Wang et al., 2017; Calvert et al., 2019; Song et al., 2019). The continuous development of techniques for stimulating and manipulating neural activity (especially in neuroscience and electronics) is expected to lead to successful therapies involving the new generation of EES strategies, and allowing voluntary control of locomotion to be restored after SCI. Our study introduces an EES protocol using three relatively distributed hotspot electrodes and burst stimulations. This EES protocol effectively restored the motor ability of hindlimbs in a complete SCI rat model. We expect that this protocol will be used in the future in investigations of evidence-based EES strategies that improve locomotion control ability without involving complex stimulation protocols.

**Acknowledgments:** *The authors would like to thank Professor Xu Qi from School of Artificial Intelligence and Automation, Huazhong University of Science and Technology, China for her technical support.*

**Author contributions:** *Study concept and design: SW, XRJ and PFT; data acquisition and statistical analysis: GXX, HTF and JHD; manuscript writing: SW and TL; manuscript editing: LCZ and XRJ; revision for intellectual content: LCZ and PFT. All authors approved the final version of the paper.*

**Conflicts of interest:** *The authors declare that there are no conflicts of interest associated with this manuscript.*

**Financial support:** *This study was supported by the National Natural Science Foundation of China, Nos. 81601052 (to XRJ), 81520108017 (to PFT); the Beijing Nova Program of Science and Technology of China, No. 2018034 (to XRJ); the Beijing Municipal Science and Technology Project of China, No. D16100002816005 (to PFT); the Subsidiary of PLA Major Project of China, No. AWS17J004 (to PFT). The funding sources had no role in study conception and design, data analysis or interpretation, paper writing or deciding to submit this paper for publication.*

**Institutional review board statement:** *This study was approved by the Animal Ethics Committee of Chinese PLA General Hospital (approval No. 2019-X15-39) on April 19, 2019. The experimental procedure followed the United States National Institutes of Health Guide for the Care and Use of Laboratory Animals (NIH Publication No. 85-23, revised 1996).*

**Copyright license agreement:** *The Copyright License Agreement has been signed by all authors before publication.*

**Data sharing statement:** *Datasets analyzed during the current study are available from the corresponding author on reasonable request.*

**Plagiarism check:** *Checked twice by iThenticate.*

**Peer review:** *Externally peer reviewed.*

**Open access statement:** *This is an open access journal, and articles are distributed under the terms of the Creative Commons Attribution-Non-Commercial-ShareAlike 4.0 License, which allows others to remix, tweak, and build upon the work non-commercially, as long as appropriate credit is given and the new creations are licensed under the identical terms.*

**Open peer reviewer:** *Linard Filli, University Hospital Zurich, Switzerland.*

**Additional file:** *Open peer review report 1.*

## References

- Anderson KD (2004) Targeting recovery: priorities of the spinal cord-injured population. *J Neurotrauma* 21:1371-1383.
- Anderson MA, O'Shea TM, Burda JE, Ao Y, Barlatay SL, Bernstein AM, Kim JH, James ND, Rogers A, Kato B, Wollenberg AL, Kawaguchi R, Coppola G, Wang C, Deming TJ, He Z, Courtine G, Sofroniew MV (2018) Required growth facilitators propel axon regeneration across complete spinal cord injury. *Nature* 561:396-400.
- Angeli CA, Edgerton VR, Gerasimenko YP, Harkema SJ (2014) Altering spinal cord excitability enables voluntary movements after chronic complete paralysis in humans. *Brain* 137:1394-1409.
- Angeli CA, Boakye M, Morton RA, Vogt J, Benton K, Chen Y, Ferreira CK, Harkema SJ (2018) Recovery of over-ground walking after chronic motor complete spinal cord injury. *N Engl J Med* 379:1244-1250.

- Assinck P, Duncan GJ, Hilton BJ, Plemel JR, Tetzlaff W (2017) Cell transplantation therapy for spinal cord injury. *Nat Neurosci* 20:637-647.
- Badhiwala JH, Wilson JR, Fehlings MG (2019) Global burden of traumatic brain and spinal cord injury. *Lancet Neurol* 18:24-25.
- Badner A, Siddiqui AM, Fehlings MG (2017) Spinal cord injuries: how could cell therapy help? *Expert Opin Biol Ther* 17:529-541.
- Balki M, Malavade A, Ye XY, Tharmaratnam U (2019) Epidural electrical stimulation test versus local anesthetic test dose for thoracic epidural catheter placement: a prospective observational study. *Can J Anaesth* 66:380-387.
- Bamford JA, Putman CT, Mushahwar VK (2005) Intraspinal microstimulation preferentially recruits fatigue-resistant muscle fibres and generates gradual force in rat. *J Physiol* 569:873-884.
- Borrell JA, Frost SB, Peterson J, Nudo RJ (2017) A 3D map of the hindlimb motor representation in the lumbar spinal cord in Sprague Dawley rats. *J Neural Eng* 14:016007.
- Calvert JS, Grahn PJ, Zhao KD, Lee KH (2019) Emergence of epidural electrical stimulation to facilitate sensorimotor network functionality after spinal cord injury. *Neuromodulation* 22:244-252.
- Capogrosso M, Wenger N, Raspopovic S, Musienko P, Beauparlant J, Bassi Luciani L, Courtine G, Micera S (2013) A computational model for epidural electrical stimulation of spinal sensorimotor circuits. *J Neurosci* 33:19326-19340.
- Capogrosso M, Wagner FB, Gandar J, Moraud EM, Wenger N, Milekovic T, Shkorbatova P, Pavlova N, Musienko P, Bezdar E, Bloch J, Courtine G (2018) Configuration of electrical spinal cord stimulation through real-time processing of gait kinematics. *Nat Protoc* 13:2031-2061.
- Cofano F, Boido M, Monticelli M, Zenga F, Ducati A, Vercelli A, Garbossa D (2019) Mesenchymal stem cells for spinal cord injury: current options, limitations, and future of cell therapy. *Int J Mol Sci* 20:E2698.
- Collaborators GBDN (2019) Global, regional, and national burden of neurological disorders, 1990-2016: a systematic analysis for the Global Burden of Disease Study 2016. *Lancet Neurol* 18:459-480.
- Courtine G, Song B, Roy RR, Zhong H, Herrmann JE, Ao Y, Qi J, Edgerton VR, Sofroniew MV (2008) Recovery of supraspinal control of stepping via indirect propriospinal relay connections after spinal cord injury. *Nat Med* 14:69-74.
- Danner SM, Hofstoetter US, Freundl B, Binder H, Mayr W, Rattay F, Minassian K (2015) Human spinal locomotor control is based on flexibly organized burst generators. *Brain* 138:577-588.
- Darrow D, Balser D, Netroff TI, Krassioukov A, Phillips A, Parr A, Samadani U (2019) Epidural spinal cord stimulation facilitates immediate restoration of dormant motor and autonomic supraspinal pathways after chronic neurologically complete spinal cord injury. *J Neurotrauma* 36:2325-2336.
- David G, Mohammadi S, Martin AR, Cohen-Adad J, Weiskopf N, Thompson A, Freund P (2019) Traumatic and nontraumatic spinal cord injury: pathological insights from neuroimaging. *Nat Rev Neurol* 15:718-731.
- Eckert MJ, Martin MJ (2017) Trauma: spinal cord injury. *Surg Clin North Am* 97:1031-1045.
- Edgerton VR, Courtine G, Gerasimenko YP, Lavrov I, Ichihama RM, Fong AJ, Cai LL, Otsuchi CK, Tillakaratne NJ, Burdick JW, Roy RR (2008) Training locomotor networks. *Brain Res* 57:241-254.
- Epstein LJ, Palmieri M (2012) Managing chronic pain with spinal cord stimulation. *Mt Sinai J Med* 79:123-132.
- Flynn JR, Bolton PS (2007) Measurement of the vertebral canal dimensions of the neck of the rat with a comparison to the human. *Anat Rec (Hoboken)* 290:893-899.
- Formento E, Minassian K, Wagner F, Mignardot JB, Le Goff-Mignardot CG, Rowald A, Bloch J, Micera S, Capogrosso M, Courtine G (2018) Electrical spinal cord stimulation must preserve proprioception to enable locomotion in humans with spinal cord injury. *Nat Neurosci* 21:1728-1741.
- Gerasimenko YP, Lavrov IA, Courtine G, Ichihama RM, Dy CJ, Zhong H, Roy RR, Edgerton VR (2006) Spinal cord reflexes induced by epidural spinal cord stimulation in normal awake rats. *J Neurosci Methods* 157:253-263.
- Gerasimenko YP, Ichihama RM, Lavrov IA, Courtine G, Cai L, Zhong H, Roy RR, Edgerton VR (2007) Epidural spinal cord stimulation plus quipazine administration enable stepping in complete spinal adult rats. *J Neurophysiol* 98:2525-2536.
- Gill ML, Grahn PJ, Calvert JS, Linde MB, Lavrov IA, Strommen JA, Beck LA, Sayenko DG, Van Straaten MG, Drubach DI, Veith DD, Thoreson AR, Lopez C, Gerasimenko YP, Edgerton VR, Lee KH, Zhao KD (2018) Neuromodulation of lumbosacral spinal networks enables independent stepping after complete paraplegia. *Nat Med* 24:1677-1682.
- Gonzalez AA, Shilian P, Hsieh P (2013) Spinal cord mapping. *J Clin Neurophysiol* 30:604-612.
- Harkema S, Gerasimenko Y, Hodes J, Burdick J, Angeli C, Chen Y, Ferreira C, Willhite A, Rejc E, Grossman RG, Edgerton VR (2011) Effect of epidural stimulation of the lumbosacral spinal cord on voluntary movement, standing, and assisted stepping after motor complete paraplegia: a case study. *Lancet* 377:1938-1947.
- Hunter JP, Ashby P (1994) Segmental effects of epidural spinal cord stimulation in humans. *J Physiol* 474:407-419.
- Hutson TH, Di Giovanni S (2019) The translational landscape in spinal cord injury: focus on neuroplasticity and regeneration. *Nat Rev Neurol* 15:732-745.
- Jackson A (2016) Spinal-cord injury: Neural interfaces take another step forward. *Nature* 539:177-178.
- Jackson A, Zimmermann JB (2012) Neural interfaces for the brain and spinal cord—restoring motor function. *Nat Rev Neurol* 8:690-699.
- Jaumard NV, Leung J, Gokhale AJ, Guarino BB, Welch WC, Winkelstein BA (2015) Relevant anatomic and morphological measurements of the rat spine: considerations for rodent models of human spine trauma. *Spine (Phila Pa 1976)* 40:E1084-1092.
- Kapur L, Deer T, Yakovlev A, Bensitel T, Hayek S, Pyles S, Khan Y, Kapural A, Cooper D, Stearns L, Zovkic P (2010) Technical aspects of spinal cord stimulation for managing chronic visceral abdominal pain: the results from the national survey. *Pain Med* 11:685-691.
- Karunakaran KD, He J, Zhao J, Cui JL, Zang YF, Zhang Z, Biswal BB (2019) Differences in cortical gray matter atrophy of paraplegia and tetraplegia after complete spinal cord injury. *J Neurotrauma* 36:2045-2051.
- Kim HY, Kumar H, Jo MJ, Kim J, Yoon JK, Lee JR, Kang M, Choo YW, Song SY, Kwon SP, Hyeon T, Han IB, Kim BS (2018) Therapeutic efficacy-potentiated and diseased organ-targeting nanovesicles derived from mesenchymal stem cells for spinal cord injury treatment. *Nano Lett* 18:4965-4975.
- Kjell J, Olson L (2016) Rat models of spinal cord injury: from pathology to potential therapies. *Dis Model Mech* 9:1125-1137.
- Koffler J, Zhu W, Qu X, Platoshyn O, Dulin JN, Brock J, Graham L, Lu P, Sakamoto J, Marsala M, Chen S, Tuszynski MH (2019) Biomimetic 3D-printed scaffolds for spinal cord injury repair. *Nat Med* 25:263-269.
- Lavrov I, Dy CJ, Fong AJ, Gerasimenko Y, Courtine G, Zhong H, Roy RR, Edgerton VR (2008) Epidural stimulation induced modulation of spinal locomotor networks in adult spinal rats. *J Neurosci* 28:6022-6029.
- Li X, Liu D, Xiao Z, Zhao Y, Han S, Chen B, Dai J (2019) Scaffold-facilitated locomotor improvement post complete spinal cord injury: Motor axon regeneration versus endogenous neuronal relay formation. *Biomaterials* 197:20-31.
- Mohan R, Tosolini AP, Morris R (2015) Segmental distribution of the motor neuron columns that supply the rat hindlimb: a muscle/motor neuron tract-tracing analysis targeting the motor end plates. *Neuroscience* 307:98-108.
- Moir L (2009) Managing chronic neuropathic pain: the role of spinal cord stimulation. *Br J Community Nurs* 14:207-209.
- Moritz CT, Lucas TH, Perlmutter SI, Fetz EE (2007) Forelimb movements and muscle responses evoked by microstimulation of cervical spinal cord in sedated monkeys. *J Neurophysiol* 97:110-120.
- Mushahwar VK, Aoyagi Y, Stein RB, Prochazka A (2004) Movements generated by intraspinal microstimulation in the intermediate gray matter of the anesthetized, decerebrate, and spinal cat. *Can J Physiol Pharmacol* 82:702-714.
- Ni S, Luo Z, Jiang L, Guo Z, Li P, Xu X, Cao Y, Duan C, Wu T, Li C, Lu H, Hu J (2019) UTX/KDM6A Deletion promotes recovery of spinal cord injury by epigenetically regulating vascular regeneration. *Mol Ther* 27:2134-2146.
- Padmanabhan R, Singh S (1979) Observations on the topographical relations of spinal nerve roots in the rat. *Acta Anat (Basel)* 105:378-380.
- Panjabi MM, Takata K, Goel V, Federico D, Oxlund T, Duranceau J, Krag M (1991) Thoracic human vertebrae. Quantitative three-dimensional anatomy. *Spine (Phila Pa 1976)* 16:888-901.
- Rattay F, Minassian K, Dimitrijevic MR (2000) Epidural electrical stimulation of posterior structures of the human lumbosacral cord: 2. quantitative analysis by computer modeling. *Spinal Cord* 38:473-489.
- Ren ZW, Zhou JG, Xiong ZK, Zhu FZ, Guo XD (2019) Effect of exosomes derived from MiR-133b-modified ADSCs on the recovery of neurological function after SCI. *Eur Rev Med Pharmacol Sci* 23:52-60.
- Saltiel P, Wyler-Duda K, D'Avella A, Tresch MC, Bizzi E (2001) Muscle synergies encoded within the spinal cord: evidence from focal intraspinal NMDA iontophoresis in the frog. *J Neurophysiol* 85:605-619.
- Schiavone G, Wagner F, Fallegger F, Kang X, Vachicouras N, Barra B, Capogrosso M, Bloch J, Courtine G, Lacombe SP (2018) Long-term functionality of a soft electrode array for epidural spinal cord stimulation in a minipig model. *Conf Proc IEEE Eng Med Biol Soc* 2018:1432-1435.
- Sharpe AN, Jackson A (2014) Upper-limb muscle responses to epidural, subdural and intraspinal stimulation of the cervical spinal cord. *J Neural Eng* 11:016005.
- Shi X, Liu JS, Wan R, Wang YS (2020) Research progress in mesenchymal stem cells for treating spinal cord injury. *Zhongguo Zuzhi Gongcheng Yanjiu* 24:4081-4087.
- Song P, Cuellar CA, Tang S, Islam R, Wen H, Huang C, Manduca A, Trzasko JD, Knudsen BE, Lee KH, Chen S, Lavrov IA (2019) Functional ultrasound imaging of spinal cord hemodynamic responses to epidural electrical stimulation: a feasibility study. *Front Neurol* 10:279.
- Sun W, Larson MJ, Kiyoshi CM, Annett AJ, Stalker WA, Peng J, Tedeschi A (2019) Gabapentinoid treatment promotes corticospinal plasticity and regeneration following murine spinal cord injury. *J Clin Invest* 130:345-358.
- Sunshine MD, Cho FS, Lockwood DR, Fecko AS, Kasten MR, Moritz CT (2013) Cervical intraspinal microstimulation evokes robust forelimb movements before and after injury. *J Neural Eng* 10:036001.
- Tsintou M, Dalamagkas K, Makris N (2020) Taking central nervous system regenerative therapies to the clinic: curing rodents versus nonhuman primates versus humans. *Neural Regen Res* 15:425-437.
- Urbani MA, Royston DA, Weber DJ, Boninger ML, Collinger JL (2019) What is the functional relevance of reorganization in primary motor cortex after spinal cord injury? *Neurobiol Dis* 121:286-295.
- van den Brand R, Heutschi J, Barraud Q, DiGiovanna J, Bartholdi K, Huerlimann M, Friedli L, Vollenweider I, Moraud EM, Duis S, Dominici N, Micera S, Musienko P, Courtine G (2012) Restoring voluntary control of locomotion after paralyzing spinal cord injury. *Science* 336:1182-1185.
- Wagner FB, Mignardot JB, Goff-mignardot CG (2018) Targeted neurotechnology restores walking in humans with spinal cord injury. *Nature* 563:65-71.
- Wang X, Chaudhry SA, Hou W, Jia X (2017) Developing and evaluating a flexible wireless microcoil array based integrated interface for epidural cortical stimulation. *Int J Mol Sci* 18:E335.
- Wenger N, Moraud EM, Raspopovic S, Bonizzato M, DiGiovanna J, Musienko P, Morari M, Micera S, Courtine G (2014) Closed-loop neuromodulation of spinal sensorimotor circuits controls refined locomotion after complete spinal cord injury. *Sci Transl Med* 6:255ra133.
- Wenger N, Moraud EM, Gandar J (2016) Spatiotemporal neuromodulation therapies engaging muscle synergies improve motor control after spinal cord injury. *Nat Med* 22:138-145.
- Yokota K, Kubota K, Kobayakawa K, Saito T, Hara M, Kijima K, Maeda T, Katoh H, Ohkawa Y, Nakashima Y, Okada S (2019) Pathological changes of distal motor neurons after complete spinal cord injury. *Mol Brain* 12:4.
- Young W (2015) Electrical stimulation and motor recovery. *Cell Transplant* 24:429-446.
- Yuan XN, Liang WD, Zhou FH, Li HT, Zhang LX, Zhang ZQ, Li JJ (2019) Comparison of walking quality variables between incomplete spinal cord injury patients and healthy subjects by using a footscan plantar pressure system. *Neural Regen Res* 14:354-360.
- Zhang W, Zhu XQ, Zhang DC (2016) Transplantation of bone marrow mesenchymal stem cells overexpressing Shootin1 for treatment of spinal cord injury. *Zhongguo Zuzhi Gongcheng Yanjiu* 20:7507-7517.
- Zheng Y, Mao YR, Yuan TF, Xu DS, Cheng LM (2020) Multimodal treatment for spinal cord injury: a sword of neuroregeneration upon neuromodulation. *Neural Regen Res* 15:1437-1450.
- Zhou H, Xu Q, He J, Ren H, Zhou H, Zheng K (2012) A fully implanted programmable stimulator based on wireless communication for epidural spinal cord stimulation in rats. *J Neurosci Methods* 204:341-348.

P-Reviewer: Filli L; C-Editor: Zhao M; S-Editors: Wang J, Li CH; L-Editors: Gardner B, Pack M, Qiu Y, Song LP; T-Editor: Jia Y